KRITTIKA SUMMER PROJECTS 2024

Demystifying Radio Astronomy

Saatwik Patnaik

KRITTIKA SUMMER PROJECTS 2024

Demystifying Radio Astronomy

Saatwik Patnaik[1]

[1]Indian Institute of Technology, Bombay

PUBLISHED BY KRITTIKA: THE ASTRONOMY CLUB OF IIT BOMBAY
GITHUB.COM/KRITTIKAIITB
First Release, August 2024

Abstract

Radio astronomy is a sub field of astronomy that studies celestial objects at radio frequencies. Radio waves penetrate dust clouds, providing insights into regions of space that optical telescopes cannot observe, thus expanding our understanding of the universe. This project starts off with a brief introduction to radio astronomy and some basic concepts useful in making astronomical observations. It then delves into the theory behind radiation physics particularly black body radiation and how to find the temperature of celestial objects. The project highlights the significance of the 21 cm hydrogen spectral line and how it holds the key to unlocking the oldest secrets of the universe. Afterwards, we also cover some more advanced concepts used in radio telescopes to maximize their capability. In later sections, we delved into the underlying principles behind imaging radio telescope data using CASA (Common Astronomy Software Applications). The report describes various techniques to analyze and interpret data obtained from radio telescopes using CASA functions. Last but not the least, the report covers the theory behind MCMC sampling and how it enables us to fit complex models and extract reliable parameter estimates.

Contents

Index 39

Part One

1. Introduction to Radio Astronomy

1.1 Evolution over the years

The study of electromagnetism in the 1800s, particularly in the form of Maxwell's equations(4), set up the discovery of radio astronomy in the 1900s. The development of radio astronomy firstly required the amplification of radio signals entering the antenna. This was accomplished by Karl Jansky, in December 1932, when he was was able to detect astronomical radio emission. Using a steerable antenna and converting the amplified radio waves to audible sound waves, he was able to discover that the direction of the hiss was fixed relative to the stars and was coming from the plane of the galaxy. Inspired by this, Grote Reber, an engineer, built his own 30 foot antenna and succeeded in mapping the radio emission from the galaxy with a greater resolution. His findings also led to the discovery of the constellation Cassiopeia and the radio galaxy Cygnus A.
A major avenue for the study of the universe using radio observations opened up when Dutch astrophysicist Jan Oort suggested to Hendrik van de Hulst that he calculate the wavelength of the emission line of hydrogen due to the spin flip of the electron. The first detection of this 21-cm line was then made in 1951 by Harold Ewen and Edward Purcell at Harvard University. The 21-cm line is still used extensively to map the distribution of hydrogen atoms throughout space.
In 1946, Sir Martin Ryle and D. D. Vonberg made the first astronomical observation using a pair of radio antennas as an interferometer, marking the first step in the long development of a high-resolution radio astronomy observing technique.
In the 1950s, Hannes Alfvén and Nicolai Herlofsen, in Sweden, and Iosif Shklovsky, in Russia, theorized that the continuum radio emission from the most intense radio sources results from an exotic process known as synchrotron radiation, in which relativistic electrons emit photons as they spiral around magnetic field lines. During the 1960s, radio astronomy yielded discoveries of quasars, pulsars, and the cosmic microwave background.

1.2 A Brief Overview

Radio waves are a form of electromagnetic radiation which means that it consists of pair of mutually perpendicular oscillating electric and magnetic fields. EM waves are created when charged particles undergo acceleration. The wavelength, frequency and speed of these waves are related by:

$$\lambda f = c \tag{1.1}$$

The oscillating electric and magnetic fields give us the wave nature of light. However light can also be described as a massless particle known as photon having energy E given by:

$$E = hv = \frac{hc}{\lambda} \tag{1.2}$$

where h is the Planck constant.
Different energy, frequency and wavelengths together give us the electromagnetic spectrum where the radio window ranges from 10MHz to 300GHz. This large range of frequencies can travel through the Earth's atmosphere unimpeded and thus provides an excellent realm for the detection and study of EM radiation from space.

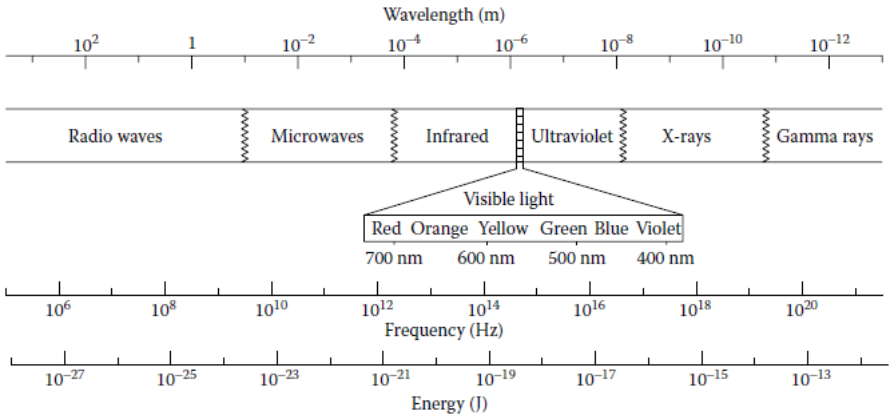

Figure 1.1: Electromagnetic Spectrum

1.2.1 Spectroscopy

A powerful tool for analyzing the detected radiation is to examine its spectrum (a plot of the amount of radiation vs. frequency or wavelength). There are three general types of spectra, as described by Kirchhoff's rules.

- **Continuous spectra**: When a radiation source emits at all frequencies over a range without breaks, the spectrum is called a continuous spectrum and the emitting object is called a continuum source.
- **Bright line or emission line spectra**: When a radiating object emits radiation only at some specific frequencies, or wavelengths, the spectrum contains a set of discrete bright lines. These lines of light are called emission lines and are emitted due to the quantum physics of atomic and molecular structures. Different atoms and molecules emit different sets of frequencies, and so the composition of a radiation source can be identified by determining the frequencies of the emission lines.

- **Dark line or absorption line spectra**: When the radiation from an intense continuum source passes through a cool, transparent gas of atoms or molecules, the spectrum on the other side will show the continuous spectrum of the background source with the radiation at specific frequencies appearing darkened. These regions are called absorption lines and occur when some of the atoms or molecules in the gas absorb photons from the continuum to raise them into a higher allowed energy level.

1.3 Sky Coordinate System

The equatorial system is a celestial coordinate system commonly used in astronomy to locate celestial objects on the celestial sphere. It provides a consistent reference frame that remains fixed with respect to the stars, allowing astronomers to accurately determine the positions of objects regardless of Earth's rotation. The celestial sphere is imagined as a globe of the sky, with a globe of Earth at its center. The poles of the celestial sphere (north and south) are the points directly overhead the poles on Earth. Similarly the extension of the Earth's equator on this sphere is known as the celestial equator.
Extensions of the lines of longitude on Earth produce similar lines on the sky, known as lines of right ascension (RA), denoted by α. Similarly, extensions of the lines of latitude make lines on the sky called declination (Dec), denoted by δ. The angles defined using these lines are fundamental in determining the position of an object in the sky.
Additionally it is also important to note that the angular separation between adjacent longitude lines depends on the latitude where the separation is measured i.e, the angular separation of two RA lines is proportional to the cosine of DEC. Thus RA is measured in units of time and DEC in degrees, because the displacement between RA lines and longitude lines is related to the rotation of Earth. general relation between the number seconds of RA and seconds of arc is given by:

$$\text{Seconds of arc} = 15\cos(\delta) \times \text{Seconds of RA}$$

where δ is the DEC.

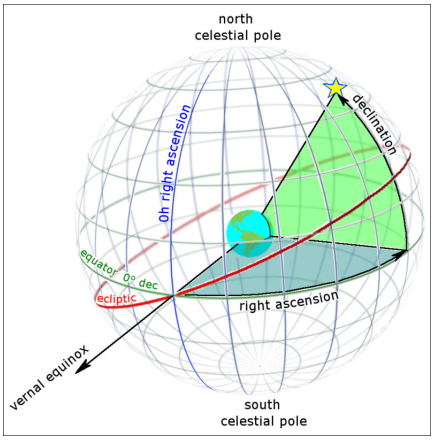

Figure 1.2: Right Ascension and Declination

1.3.1 Observer-Centered Definitions

- **Horizon**: Defines the limit of what parts of the sky you can see at any particular moment taking into account the ground and structures on Earth blocking your view of the sky.
- **Zenith**: Defines the point in the sky directly overhead which changes continuously (unless standing at the poles) due to rotation of Earth.
- **Altitude or elevation**: Defines the angular height of an object above your horizon at any given moment. When a star is just rising or just setting, its altitude, or elevation, is 0°, and when it is directly overhead—at the zenith—its altitude, or elevation, is 90°.
- **Azimuth**: This is the angular position perpendicular to the altitude, and is defined as the angular position of an object along the horizon relative to due north.
- **Meridian**: This is the line of RA that runs through your zenith. Equivalently, it is the line in the sky that runs through both your zenith and the celestial poles.
- **Transit**: This means to pass through the meridian. This is basically the midpoint of the time that an object is visible above the horizon (i.e., the moment in time halfway between rising and setting).
- **Hour angle (HA)**: An object's HA is the amount of time (in hours) since the object transited.
- **Local sidereal time (LST)**: This is defined as the RA of the meridian. If we know the LST, we can calculate the object's HA using:

$$HA = LST - RA \tag{1.3}$$

- **Universal time (UT)**: This is the solar time (time measured using period between transits of the sun) in Greenwich, England (i.e., the time on the clock where the longitude is 0°). This is useful for marking the exact time of an observation or an event. Universal time is particularly useful for situations in which the different time zones can cause confusion.

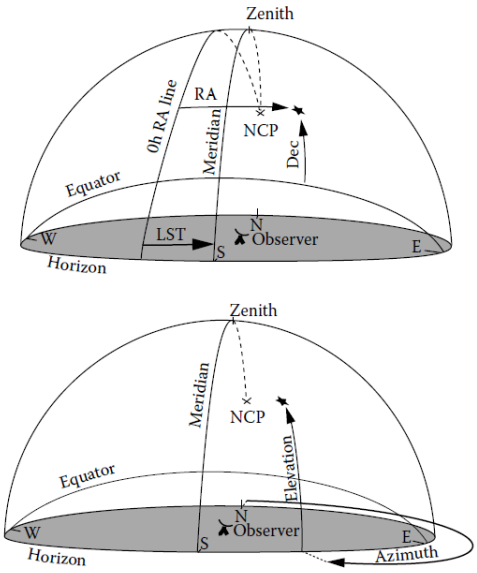

Figure 1.3: Sky coordinates as viewed by the observer

1.4 Multi wavelength astronomy

Studying the vast expanse of the universe across the electromagnetic spectrum gives us a more comprehensive understanding of the huge celestial expanse that surrounds us. X-rays and gamma rays grant insights into energetic phenomena like black holes, supernova remnants, hot gas, and neutron stars. Ultraviolet light exposes hot stars and quasars, while visible light illuminates warmer stars, planets, nebulae, and galaxies. Infrared observations unveil cool stars, regions of star formation, dusty cosmic expanses, and the heart of our galaxy. Finally, radio waves allow us to explore cold molecular clouds, help map celestial radio sources and reveal the remnants of the cosmic background radiation.
To understand this significance better, below are a few galaxy images taken in radio, infrared and visible wavelengths(1). Combing knowledge from all wavelengths thus give us a more complete and detailed picture of the galaxy.

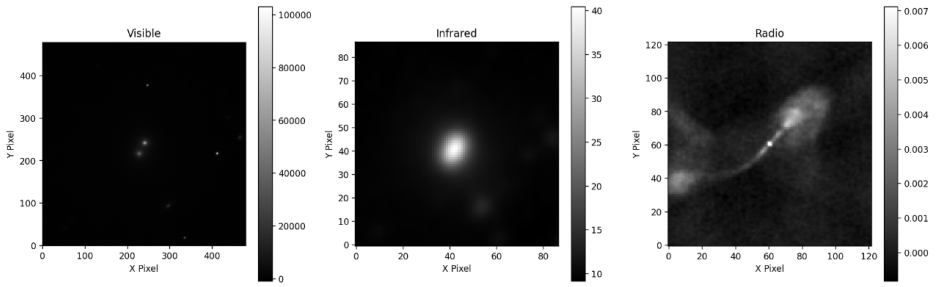

Figure 1.4: Radio galaxy NGC 0326 NED01

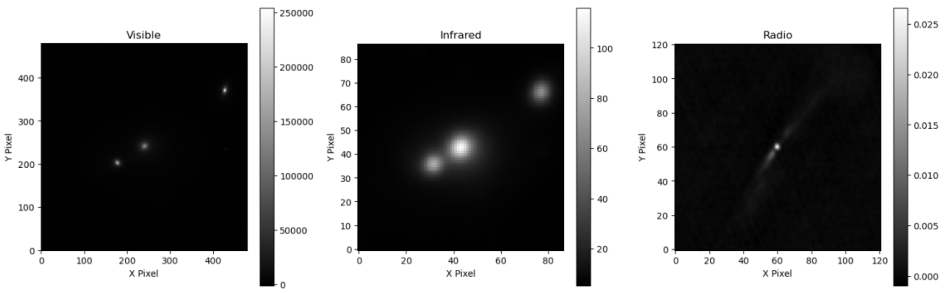

Figure 1.5: Radio galaxy NGC 1044 NED01

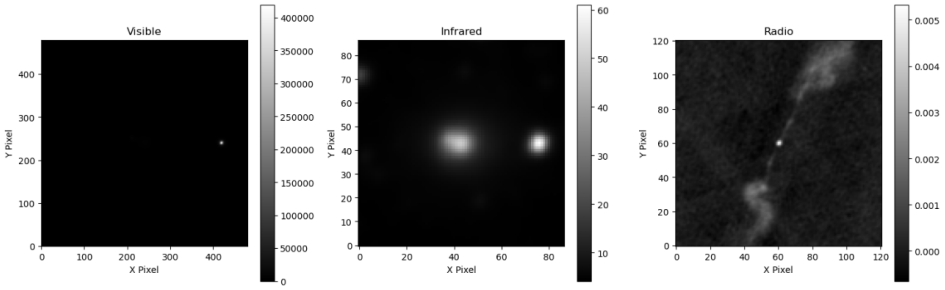

Figure 1.6: Radio galaxy VV 382 NED01

2. Jet Afterglow Lightcurve

2.1 Introduction

Neutron stars are the some of the smallest and densest objects known in the universe and are formed when a massive star runs out of fuel and collapses. When two neutron stars spiral together in binary systems, they emit gravitational waves and move closer and closer until they collide. When this happens, a flash of light in the from of gamma rays is emitted and this is known as a Gamma ray burst.
GW170817 was a gravitational wave (GW) signal observed by the LIGO and Virgo detectors on 17 August 2017, originating from the shell elliptical galaxy NGC 4993(2). The signal was produced by the last moments of the inspiral process of a binary pair of neutron stars, ending with their merger. It was the first GW observation to be confirmed by non-gravitational means. Unlike the five previous GW detections—which were of merging black holes and thus not expected to produce a detectable electromagnetic signal—the aftermath of this merger, the afterglow, was seen across the electromagnetic spectrum marking a significant breakthrough for multi-messenger astronomy.
Afterglows are considered to be an excellent cosmic laboratory for studying acceleration of particles in the cosmos, due to the apparent simplicity of the underlying physics. These can be studied by plotting the flux density (amount of energy incident on the detector per unit area of the detector), an indicator of the brightness of the source, with respect to time. Such a plot is known as a light curve. We used the data for the non-thermal emission from this source that spans across all frequency bands following a single spectral index:

$$F_\nu \propto \nu^{-0.584} \tag{2.1}$$

2.2 Plots

Plotting the lightcurve using all VLA 3GHz data points:

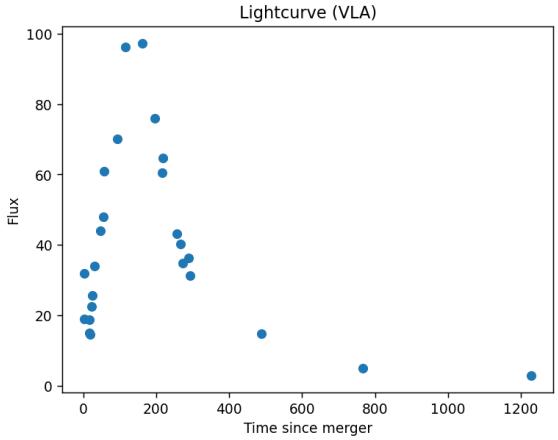

Figure 2.1: Flux density v/s time observed at 3 GHz

Now, we choose the X ray telescope Chandra which has observations of the same source at 2.41×10^{17} Hz. For all data points, we used the constant spectral index given above to scale the flux density values down to 3 GHz and then plotted this together with the VLA plot.

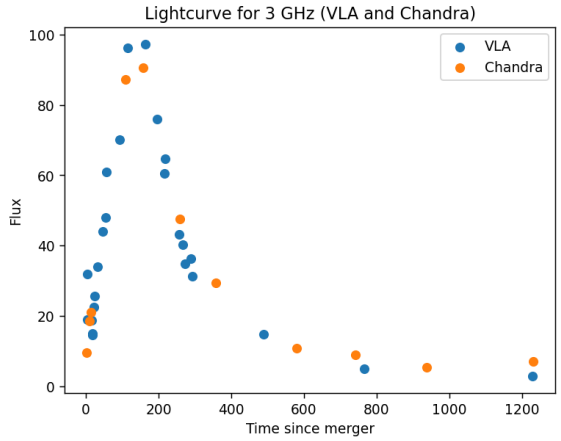

Figure 2.2: Flux density v/s time observed by Chandra and VLA telescopes scaled to 3 GHz

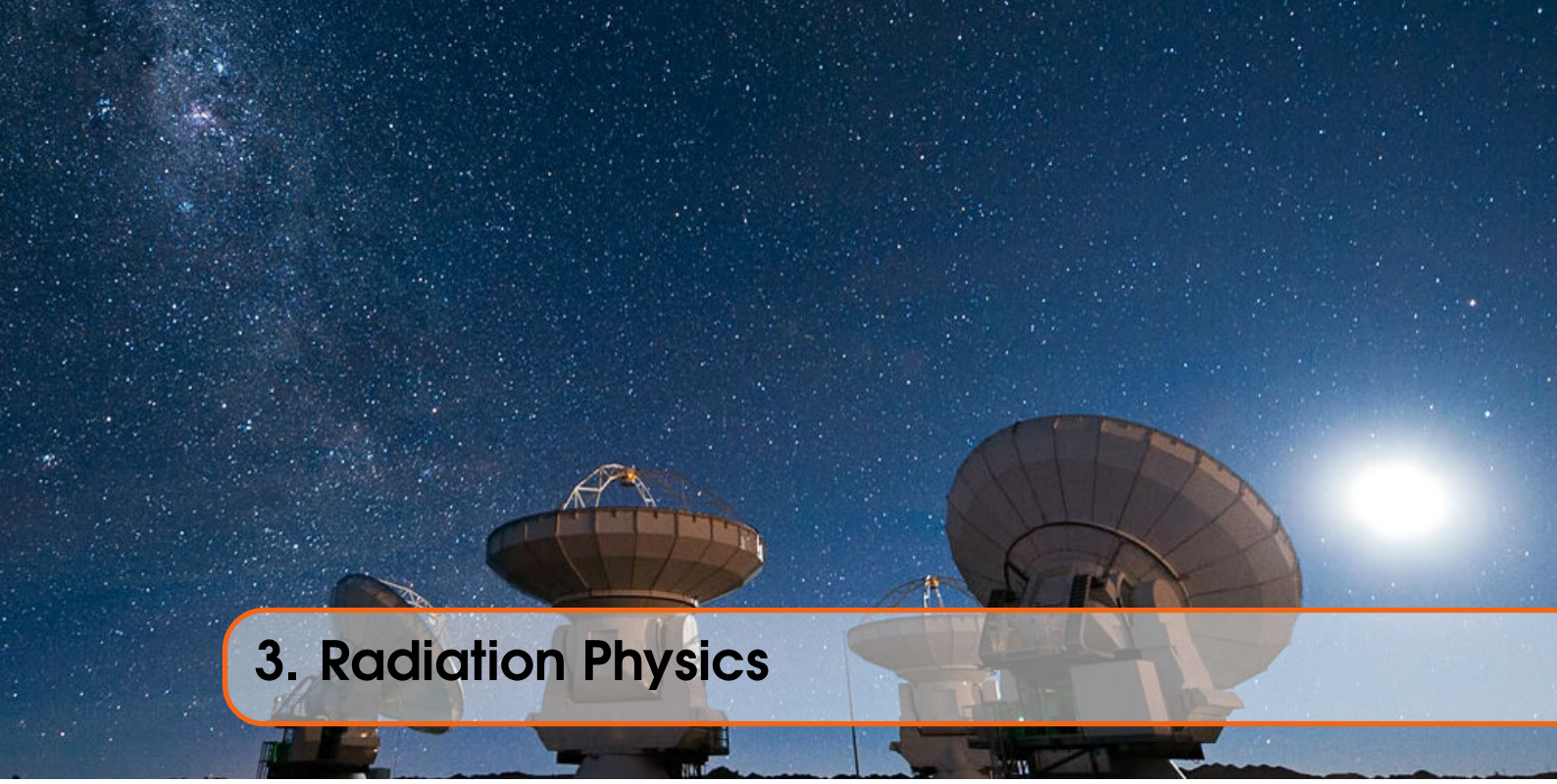

3. Radiation Physics

3.1 Measuring the amount of radiation

At radio wavelengths, astronomers measure the amount of radiation in terms of the energy recieved. Since we can only measure the total enegy emitted over a time period rather than over the entire lifetime of the source, we use a quantity known as lumiosity instead. This is the simply the energy normalized by the time period and has units of Js^{-1} or watts (W).
Luminosity, however, is not directly measurable because we do not detect all the radiation that was emitted by the source in any given second. The vast majority of the radiation is emitted in directions other than toward our telescope. Thus, we now measure flux (F), that is, the amount of light energy per unit time per unit area. The units of flux are $Js^{-1}\ m^{-2}$ or Wm^{-2} (SI). The radiation flux, that is, the detected power divided by the area of the telescope (for an isotropic source), then, is related to the luminosity of the source by:

$$F = \frac{L}{4\pi d^2} \tag{3.1}$$

Again flux, also, is not a truly measurable quantity because we cannot measure the radiation emitted at all frequencies over the entire EM spectrum. We can only detect the radiation emitted over the tiny fraction of the electromagnetic spectrum to which our detector is sensitive. So we measure the flux density (F_ν or F_λ) which is the flux per unit frequency in the observed spectral range, and it equals the detected flux divided by the width in frequency of the observation.

$$F_\nu = \frac{F}{\Delta\nu} \tag{3.2}$$

where Δv is the bandwidth.
Flux density is measured in jansky (Jy) such that 1 jansky (Jy) = $10^{-26}\ Wm^{-2}Hz^{-1}$.

The amount of power a telescope collects from a source of given flux density is given by:

$$P = F_v A_{eff} \Delta v \tag{3.3}$$

Lastly, we also define intensity (I_v or I_λ) or specific intensity, which is often referred to as surface brightness or just brightness. This is calculated as the flux density per unit solid angle. Intensity has units of $WHz^{-1}m^{-2}sr^{-1}$ (for I_v) or $Wnm^{-1}m^{-2}sr^{-1}$ (for I_λ). Some important aspects of intensity are:

- Flux density, F_v, does not distinguish between the directions that the photons come from or travel to, whereas I_v does.
- Intensity is independent of distance since flux density and solid angle have two separate dependences on distance and they cancel with one another.
- Intensity is a direct measure of the object's surface brightness, that is, the amount of energy radiated per second per unit area of the surface per unit solid angle right at the surface.

3.2 Blackbody radiation

One of the major breakthroughs in physics at the start of the twentieth century was the realization that light has characteristics of both waves and particles. Although light exhibits wave like properties such as interference and diffraction, it's energy comes in the form of quantized packets called photons. This discovery came to light when Max Planck realized that the spectrum of the radiation emitted by hot, opaque objects (black body) can be fit by a model that assumes quantized units of energy.

The amount of radiation emitted by a hot body must depend on the number of particles in the hot body—the more particles the body contains, the more photons that can be emitted in each second. But having a larger number of particles also increases the likelihood that some of the emitted photons will be absorbed by other particles in the body. Therefore, as more and more photons are created, there starts to be an exchange of energy from the photons back to the particles. We can think of the large number of photons, which are created in the body, as a second body of particles, so that there are two bodies present: the radiating matter (i.e., the atoms, molecules, or electrons) and a cloud of photons, both of which occupy the same volume. The particles in each body interact with those in the other, exchanging energy back and forth. The resultant radiation emitted from the body, then, is a cloud of photons at the same temperature as the body itself. With blackbody radiation, the photons have achieved a thermal distribution of energies and thus statistics can describe the distribution of energies of the photons. Using the Boltzmann distribution to determine the expected occupancy of the modes (different values of the wave vector) in thermal equilibrium, the probability that a single mode has energy E_n = nhv is given by the usual Boltzmann factor:

$$p(n) = \frac{e^{(-E_n/kT)}}{\sum_{n=0}^{\infty} e^{(-E_n/kT)}} \tag{3.4}$$

Now, mean energy of the mode of frequency v is:

$$\overline{E_v} = \sum_{n=0}^{\infty} E_n p(n) \tag{3.5}$$

Substituting the values and applying series expansion, we get mean energy of the mode:

$$\overline{E_v} = \frac{hv}{e^{hv/kT} - 1} \tag{3.6}$$

Using the concepts of electromagnetic wave in a box we can also show that the number of modes in the frequency interval v to v+dv is ($8\pi v^2/c^3$) dv per unit volume.
Using what we have derived, we can now define the Planck function in terms of the emitted flux per unit frequency interval per unit steradian as:

$$B_v(T) = \frac{2hv^3}{c^2} \frac{1}{e^{hv/kT} - 1} \tag{3.7}$$

Since this is an intensity, the Planck function can also be expressed as flux per unit wavelength per steradian, which is denoted as B_λ(T).

$$B_\lambda(T) = \frac{2hc^2}{\lambda^5} \frac{1}{e^{hc/\lambda kT} - 1} \tag{3.8}$$

Note: Although B_v and B_λ represent the same concept, they are not the same numerical quantity or even the same function.
The total flux of radiation (W m^{-2}) emitted by the body can be obtained by integration of the Planck function over frequency and solid angle. The result shows that the total flux is proportional to the fourth power of the body's temperature:

$$F = \sigma T^4 \tag{3.9}$$

This is known as the Stefan–Boltzmann law and the constant is known as the Stefan–Boltzmann constant (σ = 5.67$\times$ 10^{-8} $Wm^{-2}K^{-4}$).
A key feature of the blackbody radiation is that as the temperature of the blackbody increases, the value of B_v(T) increases at every frequency, meaning that a hotter body produces more energy at every frequency. The blackbody curves for different temperatures never cross. Therefore, if you know the intensity of an opaque object at only a single frequency, and if you know the radiating source is a blackbody, then you can infer the temperature of the source from the measure of that single intensity.

3.2.1 Cosmic Microwave Background

The Cosmic Microwave Background is radiation from around 400,000 years after the start of the Universe. Before this time, the Universe was so hot and dense that it was opaque to all radiation. Not even simple atoms could form without instantly being ripped apart into their constituent protons and electrons by the intense radiation. The Universe was made of a "plasma", or ionised gas, which is what the surface of the Sun is made of.
After the Big Bang, the Universe has been cooling and expanding. By around 400,000 years through its life it was cool enough for the simplest atoms to form, and it became transparent. The light from this time has been travelling through space ever since, and can be detected all around us from here on Earth or in space which means we can measure the afterglow of the Big Bang. The expansion of the Universe has stretched out the CMB radiation by around 1000 times, which makes

it look much cooler. So instead of seeing the afterglow at 3000 degrees, we see it at just 3K. Since it is so cold, the light which was emitted by the glowing Universe now has a much longer wavelength than we can see with our eyes. This can be seen from the fact that the CMB is brightest at a wavelength of around 2 mm.
In the 1990s, a satellite called COBE measured the CMB over the whole sky helping establish several things. Firstly, the CMB is almost completely uniform, with an almost constant temperature over the whole sky with few tiny ripples or fluctuations.
These small fluctuations are because of tiny variations in the density of the Universe immediately after the Big Bang. Any regions which are slightly more dense tend to attract more matter, and get even denser and attract even more material. This runaway process is what led to the formation of the first stars and galaxies. The properties of the fluctuations have been used to help determine the age of the Universe, what it's made of, and even how it might end.

Curve Fitting

Using the far infrared data adapted from the COBE satellite, we can use Planck's function to fit a blackbody radiation curve to the CMB and thus estimate its temperature. Fitting the curve gives us the temperature of the CMB as 2.74 K.

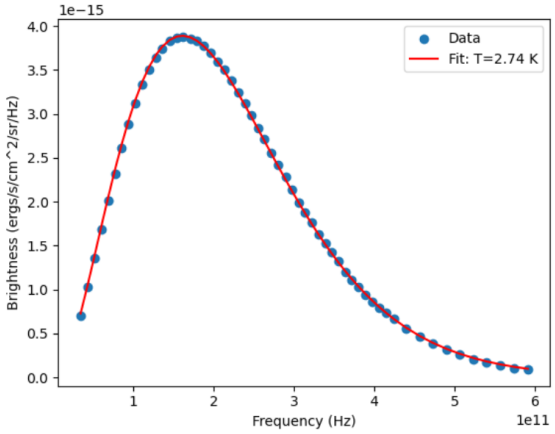

Figure 3.1: Cosmic Microwave Background Intensity v/s Frequency

4. The Hydrogen 21 cm line

4.1 Overview

The hydrogen 21 cm line is a spectral line that is created by a change in the energy state of electrically neutral hydrogen atoms. It is produced by a spin-flip transition, which means the direction of the electron's spin is reversed relative to the spin of the proton. This is a quantum state change between the two hyperfine levels of the hydrogen 1s ground state. The electromagnetic radiation producing this line has a frequency of 1420 MHz or a wavelength of around 21 cm in a vacuum.

4.2 Discovery

During the 1930s, it was noticed that there was a radio "hiss" that varied on a daily cycle and appeared to be extraterrestrial in origin. It was then observed that the radio waves seemed to propagate from the centre of the Galaxy. These discoveries were published in 1940 and were noted by Jan Oort. He then referred this to Hendrik van de Hulst who, in 1944, predicted that neutral hydrogen could produce radiation at a frequency of 1420.4058 MHz due to two closely spaced energy levels in the ground state of the hydrogen atom. After 1952 the first maps of the neutral hydrogen in the Galaxy were made, and revealed for the first time the spiral structure of the Milky Way.

4.3 Radiation Process

An atom of neutral hydrogen consists of an electron bound to a proton. The lowest stationary energy state of the bound electron is called its ground state. Both the electron and the proton have intrinsic magnetic dipole moments ascribed to their spin, whose interaction results in a slight increase in energy when the spins are parallel, and a decrease when antiparallel. Due to quantum mechanical discretization of the total angular momentum of the system only parallel and

antiparallel states are allowed.
In the ground state, the spin-flip transition between these aligned states has an energy difference of 5.87 μeV which corresponds to a wavelength of about 21 cm. This transition is highly forbidden with an extremely small transition rate of $2.9\times10^{-15}s^{-1}$, and a mean lifetime of the excited state of around 11 million years. Collisions of neutral hydrogen atoms with electrons or other atoms can help promote the emission of 21 cm photons. It is commonly observed in astronomical settings such as hydrogen clouds in our galaxy and others. Due to the uncertainty principle, its long lifetime gives the spectral line an extremely small natural width, so most broadening is due to Doppler shifts caused by bulk motion or nonzero temperature of the emitting regions.

4.4 Significance

The hydrogen line can readily penetrate clouds of interstellar cosmic dust that are opaque to visible light. Assuming that the hydrogen atoms are uniformly distributed throughout the galaxy, each line of sight through the galaxy will reveal a hydrogen line. The only difference between each of these lines is the Doppler shift that each of these lines has. Hence, by assuming circular motion, one can calculate the relative speed of each arm of our galaxy giving us rotation curve of our galaxy. It is then possible to use this curve and the velocity to determine the distance to a certain point within the galaxy.
This line has also been used indirectly to calculate the mass of galaxies, to put limits on any changes over time of the fine-structure constant, and to study the dynamics of individual galaxies. The magnetic field strength of interstellar space can be measured by observing the Zeeman effect on the 21 cm line.
Mapping the intensity of redshifted 21 centimeter radiation can, in principle, provide a very precise picture of the matter power spectrum in the period after recombination (when stable hydrogen atoms first formed). Second, it can provide a picture of how the universe was re-ionized, as neutral hydrogen which has been ionized by radiation from stars or quasars will appear as holes in the 21 cm background. Although 21 cm observations are very difficult to make, they are still generally viewed as the next great frontier in observational cosmology.

4.5 Galaxy Rotation Curve

As discussed earlier, the galaxy rotation curve can be plotted by using the doppler shifted 21 cm lines and calculating the velocity from the shifted frequency using the redshift formula. For this purpose, we will use synthetic spectra of the 21 cm line at different distances. For each distance, we will fit a gaussian to the spectrum to find the central frequency/ wavelength and then, using Doppler's effect, calculate the velocity at that distance. Plotting these velocities with respect to the distance, we obtain the galaxy rotation curve.
According to Kepler's third law, the orbital velocities of planets in planetary systems and moons orbiting planets decline with distance, as most of the mass is concentrated at the centre. The mass estimations for galaxies based on the light they emit are far too low to explain the velocity observations that the stars revolve around their galaxy's centre at equal or increasing speed over a large range of distances.

An accepted solution to this is to hypothesize the existence of dark matter and to assume its distribution from the galaxy's center out to its halo.

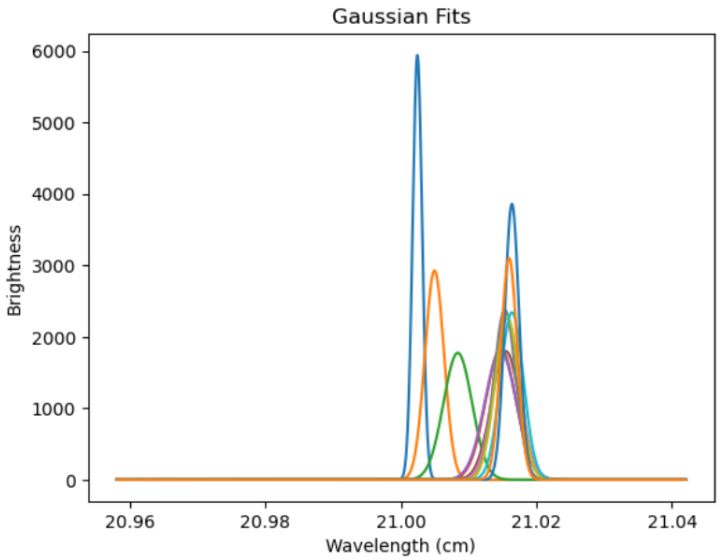

Figure 4.1: Plot of all gaussian fitted spectrums to find their central frequencies through their mean

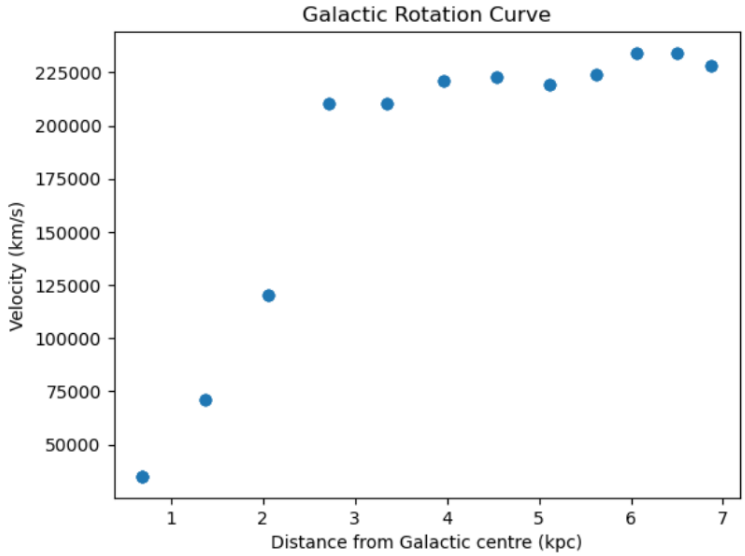

Figure 4.2: Galaxy Rotation curve

5. Radio Telescopes

5.1 Main components

5.1.1 Reflectors

The dishes of most radio telescopes are parabolic reflectors whose shape causes all waves approaching the dish from the direction perpendicular to the entrance plane to come to a single point, known as the focus of the telescope. The EM waves emitted by an astronomical object, approaching our telescope from many light years away, are well approximated as plane waves and so enter the telescope in parallel paths.

At the focal plane of a radio telescope are the feed horns, which convert the EM waves from free space to transmission lines, through which the signal travels to receivers. When the feeds (and receivers) are placed at the focus of the primary reflector, it is called a **prime focus telescope**. This configuration can be inconvenient, because the feed and receiver are in an awkward position, located high above the primary reflector and hence not easily accessible when the telescope is aimed at the sky. For this reason, most radio telescopes (and visible-light telescopes as well) are of Cassegrain design. In a **Cassegrain telescope**, a second reflector (or mirror) is placed before the focal plane of the primary reflector to redirect the waves to another focal point at or behind the vertex of the primary reflector. Most large radio telescopes are classical Cassegrain telescopes, which use a parabolic primary and hyperbolic secondary reflector.

The primary reflector serves two important functions.

- First, it collects and focuses the radiation from astronomical sources, making faint sources more detectable. The power, P, of radiation collected from an astronomical source of flux density F_ν is given by:

$$P = F_\nu A_{eff} \Delta\nu \tag{5.1}$$

- The second function of the primary reflector is to provide directivity, which is a telescope's ability to differentiate the emission from objects at different

angular positions on the sky. Directivity also determines the resolution in the map and it depends, largely, on the diameter of the primary reflector and is governed by the principle of diffraction.

5.1.2 Beam Pattern

The beam pattern is a measure of the sensitivity of the telescope to incoming radio signals as a function of angle on the sky. Ideally, we would like each feed in our telescope to collect radio signals from only one direction in the sky. Unfortunately, this is not possible due to the diffraction of light.
The behavior of light as it reflects off the primary reflector of a telescope is closely related to the behavior of light passing through a single slit. From the Huygens–Fresnel principle, the secondary waves produced at the slit interfere and add constructively or destructively depending on the position. As rays of light from an astronomical source approach the telescope, some rays reflect off the mirror and meet at the focus, while others miss the telescope and hit the ground. The reflector, thus, acts like a circular aperture.
Due to partial interference, a telescope can detect power from a source a good ways off-axis, although with much less sensitivity. As the off-axis angle increases further, the response of the telescope goes through a series of peaks and valleys. These off-axis responses are called sidelobes and are undesirable as they can add confusion to observations. The central peak of the sensitivity pattern, in contrast, is often called the main beam. measure the angular width of this peak between the two points where the received power falls to one-half of the on-axis value.

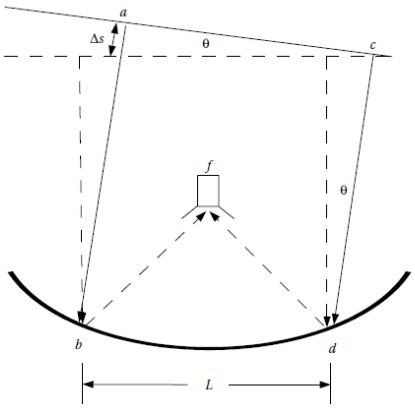

(a) Interference (for off axis source) due to path difference

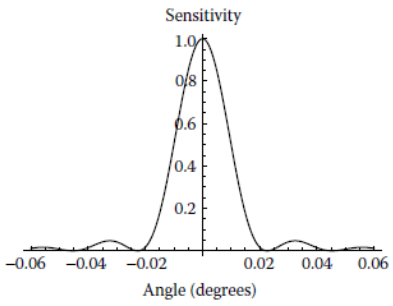

(b) Sensitivity profile for radio telescope

5.1.3 Feeds and primary reflector illumination

At the focus of a radio telescope, we need antennas to couple the EM waves in free space into waves confined to transmission lines, so that we can send the waves to the receivers. Typically, these feeds are often flared, with the radiation entering the larger end and tapering down to the proper size for a type of transmission line called a waveguide.
The minimum size of a feed horn opening at long wavelengths can be quite large, thus limiting the number of feeds that can fit in the focal plane of a radio telescope. For smaller telescopes operating at longer wavelengths, such as the Haystack

Small Radio Telescope (SRT), only one feed will fit it the focal plane, and hence the power can be measured at only one position for each pointing of the telescope. In larger telescopes, operating at millimeter and submillimeter wavelengths, an array of feeds can often be used, permitting many positions to be observed simultaneously in a single pointing.
Since radiation entering from different directions has different amounts of constructive or destructive interference, we see that the feed horn's sensitivity to radiation reflecting off different parts of the dish is necessarily nonuniform. Diffraction determines the pattern of power transmitted by the feed horn, and since the feed horn is relatively small, the power is transmitted over a large angle, illuminating the primary reflector. The beam pattern of the feed, then, determines what is known as the illumination pattern of the primary reflector.
A quantity that describes how the feed horn's beam is distributed on the primary reflector is called the edge taper, which is defined as the ratio of the sensitivity at the center of the reflector to that at the edge. This is determined by the angular width of the feed horn's beam pattern, which, like a telescope's beam pattern, is proportional to λ/D, where D, now, is the size of the large flared end of the horn. The illumination of the feed beyond the reflector is called spillover. Thus, a large edge taper optimizes the spillover efficiency, while a small edge taper optimizes the illumination efficiency. The maximum collecting area results from a compromise between spillover and illumination efficiency. The edge taper that maximizes the collecting area of the telescope is one in which the power per unit area transmitted to the center of the reflector is 10 times larger than that at the edge; this is called a 10-dB edge taper. The FWHM (for full width at half maximum) of the beam, θ_{FWHM}, with the optimum (10-dB) edge taper is

$$\theta_{FWHM} = \frac{1.15\lambda}{D} \tag{5.2}$$

5.1.4 Surface errors

The primary reflector of a radio telescope is never a perfect parabola. There are always manufacturing imperfections that limit its surface accuracy. We can characterize an imperfect reflector by the root mean square (rms) deviations, δz, of the real surface from that of an ideal parabola. Because the light is reflected off the surface, the total path difference is twice the deviation, 2δz; therefore, these deviations produce rms phase errors of $4\pi\delta$z/λ. The presence of surface errors therefore reduces the on-axis sensitivity of the telescope, and this can be viewed as a loss in the collecting area. The effect of surface errors on the collecting area is described by the Ruze equation, which is given by

$$A_\delta = A_0 e^{-(4\pi\delta z/\lambda)^2} \tag{5.3}$$

where: A_δ and A_0 are the collecting areas of a telescope with and without surface errors, respectively.

5.2 Noise, Noise Temperature and Antenna Temperature

All the components in the receiver, especially the amplifiers, generate their own electrical signals that propagate through the receiver and are unrelated to the signal from the astronomical source. This unwanted signal is known as noise.
radio astronomers also describe the power traveling in the transmission lines and receiver in terms of an equivalent temperature given by:

$$T_{equiv} = \frac{P}{k\Delta v} \tag{5.4}$$

where, k is the Boltzmann constant and Δv is the bandwidth of radiation with power P. The equivalent temperature of the power that the antenna delivers to the transmission line is called the antenna temperature, T_A. The far majority of the detected power, though, is due to noise from the receiver components. We describe the total noise power by the noise temperature, T_N, and each component in the receiver is characterized by its own noise temperature.
An amplifier's noise temperature is defined by the equivalent temperature of the noise power as if it was introduced at the input to the amplifier, and hence it is amplified along with the astronomical signal. If we have two amplifiers in succession, the first characterized by G_1 and T_{N1}, and the second by G_2 and T_{N2}, the total noise power coming out of the second amplifier is

$$P_N = G_2 G_1 k\Delta v T_{N1} + G_2 k\Delta v T_{N2} \tag{5.5}$$

Dividing by the net circuit gain and cancelling others, the total noise temperature, also known as reciever noise temperature, is

$$T_N = T_{N1} + \frac{T_{N2}}{G_1} \tag{5.6}$$

So in general, for many elements in succession, we have

$$T_N = T_{N1} + \frac{T_{N2}}{G_1} + \frac{T_{N3}}{G_1 G_2} + ... \tag{5.7}$$

The above equation shows that, the noise contribution of each successive device to the total noise is reduced by the product of the gains of the preceding elements. The RF amplifier, the first device the radiation enters into immediately after the feed, therefore, is the most critical in determining the total noise temperature.

Part Two

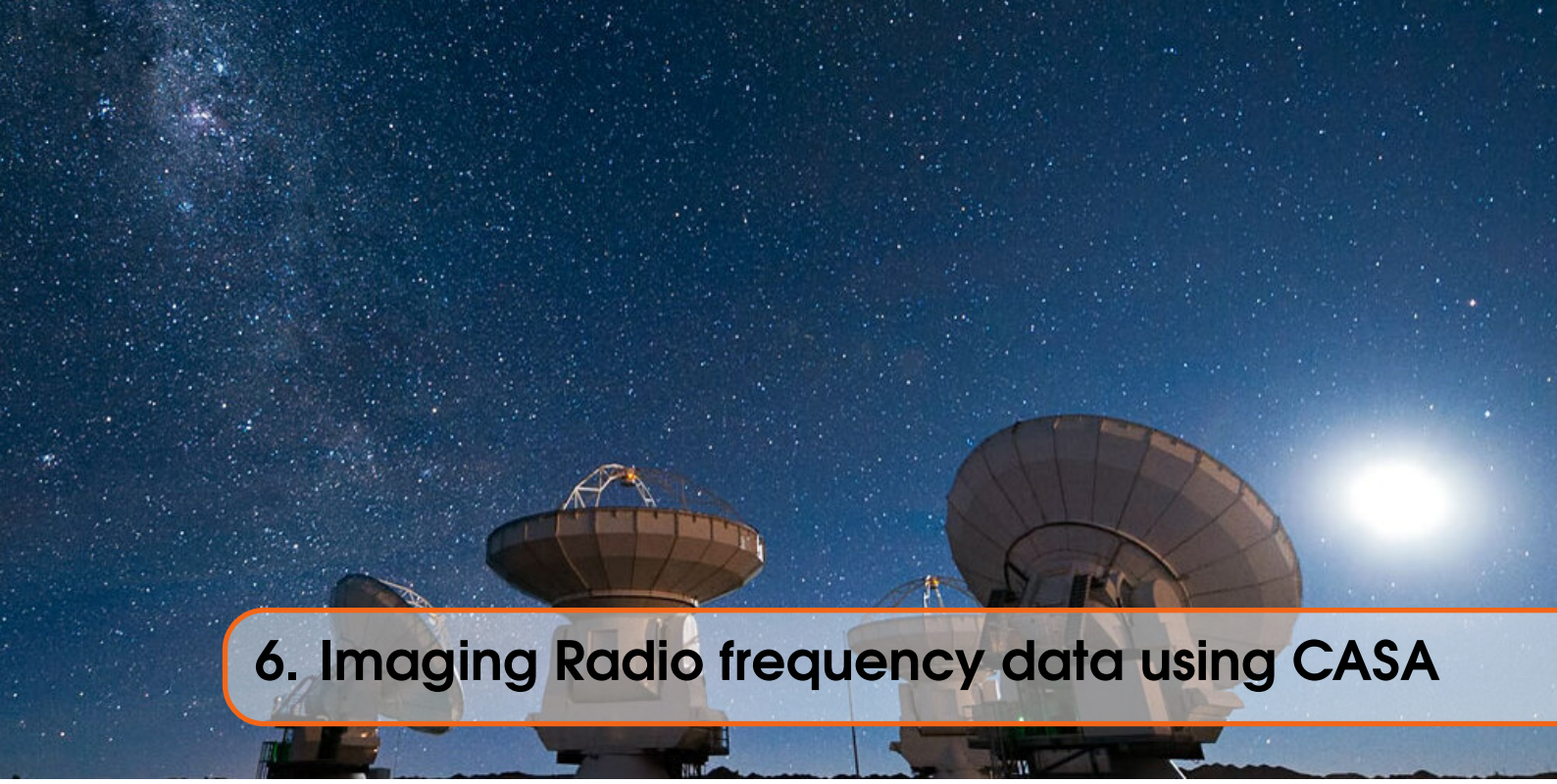

6. Imaging Radio frequency data using CASA

6.1 CASA

CASA(3) (Common Astronomy Software Applications) is a widely used software package for data reduction, calibration, and imaging in radio astronomy.

6.1.1 TW Hydra

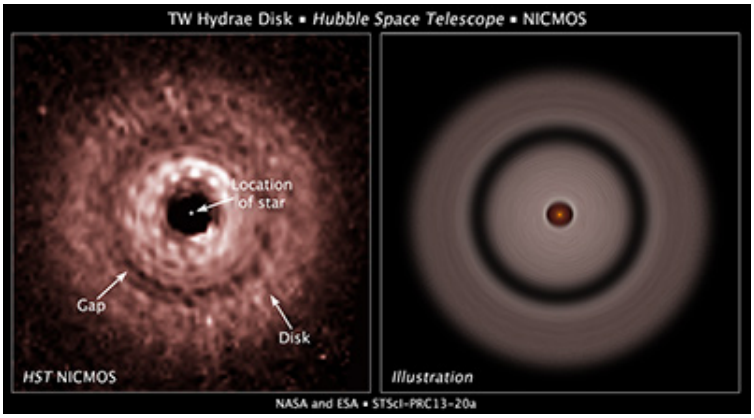

Figure 6.1: TW Hydrae protoplanetary disk

The above graphic shows a gap in a protoplanetary disk of dust and gas whirling around the nearby red dwarf star TW Hydrae.
The gap's presence is best explained as due to the effects of a growing, unseen planet that is gravitationally sweeping up material and carving out a lane in the disk.
In the NASA Hubble Space Telescope image at left, a gap can be seen about 7.5 billion miles away from the star in the center of the disk. The image was taken in

near-infrared light by the Near Infrared Camera and Multi-Object Spectrometer (NICMOS).
Astronomers used a masking device on NICMOS to block out the star's bright light so that the disk's structure could be seen. The graphic at right shows the gap relative to the star. TW Hydrae resides 176 light-years away in the constellation Hydra (the Sea Serpent). Now, our task is to image TW Hydra using CASA Software. The data which will be used for this task was obtained from the interferometer Atacama Large Millimeter Array (ALMA). Using the listobs command, we can obtain information relating to the target, a part of which is shown below.

```
CASA <1>: listobs(vis='sis14_twhya_calibrated_flagged.ms')
Out[1]:
{'BeginTime': 56250.31732611111,
 'EndTime': 56250.38269277778,
 'IntegrationTime': 5647.680000305176,
 'field_0': {'code': 'none',
  'direction': {'m0': {'unit': 'rad', 'value': 1.4092068104521434},
   'm1': {'unit': 'rad', 'value': -0.6363220835781705},
   'refer': 'J2000',
```

```
  ObservationID = 0         ArrayID = 0
Date          Timerange (UTC)          Scan  FldId FieldName             nRows    SpwIds   Average Interval(s)    ScanIntent
19-Nov-2012/07:36:57.0 - 07:39:13.1     4     0 J0522-364               4200   [0]   [6.05]  [CALIBRATE_BANDPASS#ON_SOURCE,CALIBRATE_PHASE#ON_SOURCE,CALIBRATE_WVR#ON_SOURCE]
            07:44:45.2 - 07:47:01.2     7     2 Ceres                   3800   [0]   [6.05]  [CALIBRATE_AMPLI#ON_SOURCE,CALIBRATE_PHASE#ON_SOURCE,CALIBRATE_WVR#ON_SOURCE]
            07:52:42.0 - 07:53:47.6    10     3 J1037-295               1900   [0]   [6.05]  [CALIBRATE_PHASE#ON_SOURCE,CALIBRATE_WVR#ON_SOURCE]
            07:56:23.5 - 08:02:11.3    12     5 TW Hya                  8514   [0]   [6.05]  [OBSERVE_TARGET#ON_SOURCE]
            08:04:36.3 - 08:05:41.9    14     3 J1037-295               1900   [0]   [6.05]  [CALIBRATE_PHASE#ON_SOURCE,CALIBRATE_WVR#ON_SOURCE]
            08:08:09.6 - 08:13:57.3    16     5 TW Hya                 10360   [0]   [6.05]  [OBSERVE_TARGET#ON_SOURCE]
            08:16:20.6 - 08:17:26.2    18     3 J1037-295               2100   [0]   [6.05]  [CALIBRATE_PHASE#ON_SOURCE,CALIBRATE_WVR#ON_SOURCE]
            08:19:53.9 - 08:25:41.7    20     5 TW Hya                 10321   [0]   [6.05]  [OBSERVE_TARGET#ON_SOURCE]
            08:28:17.1 - 08:29:22.6    22     3 J1037-295               2100   [0]   [6.05]  [CALIBRATE_PHASE#ON_SOURCE,CALIBRATE_WVR#ON_SOURCE]
            08:32:00.5 - 08:37:48.2    24     5 TW Hya                 10324   [0]   [6.05]  [OBSERVE_TARGET#ON_SOURCE]
            08:40:11.9 - 08:41:17.4    26     3 J1037-295               2100   [0]   [6.05]  [CALIBRATE_PHASE#ON_SOURCE,CALIBRATE_WVR#ON_SOURCE]
            08:43:45.6 - 08:49:33.4    28     5 TW Hya                  9462   [0]   [6.05]  [OBSERVE_TARGET#ON_SOURCE]
            08:51:57.1 - 08:53:02.6    30     3 J1037-295               1900   [0]   [6.05]  [CALIBRATE_PHASE#ON_SOURCE,CALIBRATE_WVR#ON_SOURCE]
            08:58:12.0 - 09:00:28.1    33     6 3c279                   3402   [0]   [6.05]  [CALIBRATE_BANDPASS#ON_SOURCE,CALIBRATE_PHASE#ON_SOURCE,CALIBRATE_WVR#ON_SOURCE]
            09:01:35.7 - 09:02:41.2    34     3 J1037-295               1900   [0]   [6.05]  [CALIBRATE_PHASE#ON_SOURCE,CALIBRATE_WVR#ON_SOURCE]
            09:05:15.6 - 09:07:31.6    36     5 TW Hya                  4180   [0]   [6.05]  [OBSERVE_TARGET#ON_SOURCE]
            09:09:59.1 - 09:11:04.7    38     3 J1037-295               2100   [0]   [6.05]  [CALIBRATE_PHASE#ON_SOURCE,CALIBRATE_WVR#ON_SOURCE]
          (nRows = Total number of rows per scan)
```

We can start inspecting the data by plotting the UV coverage, using the plotms command which allows us to look at the UV data in a graphical manner.

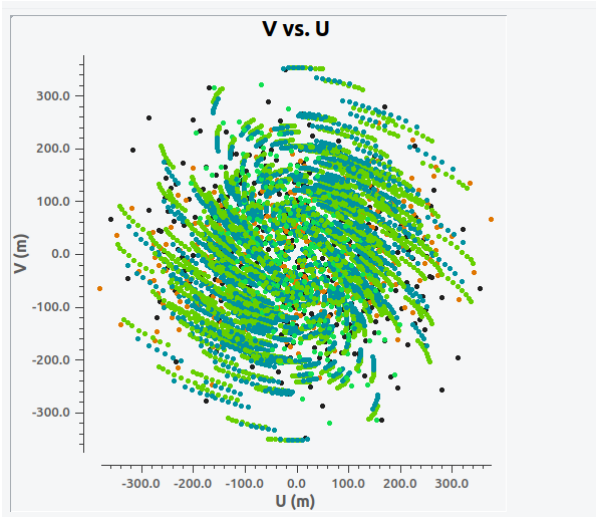

Moving onto cleaning the image, we can now use the command **tclean** in CASA. After running this in CASA, the cleaned image along with the initial dirty one is given below.
The imstat command in CASA gives an integrated flux density of about 1.512 Janskys in the region around the source.

```
CASA <4>: os.system('rm -rf phase_cal.*')
Out[4]: 0

CASA <5>: tclean(vis='sis14_twhya_calibrated_flagged.ms',
     ...:        imagename='phase_cal',
     ...:        field='3',
     ...:        spw='',
     ...:        specmode='mfs',
     ...:        deconvolver='hogbom',
     ...:        gridder='standard',
     ...:        imsize=[128,128],
     ...:        cell=['0.1arcsec'],
     ...:        weighting='briggs',
     ...:        threshold='0mJy',
     ...:        niter=5000,
     ...:        interactive=True)
```

Figure 6.2: Various parameters for tclean

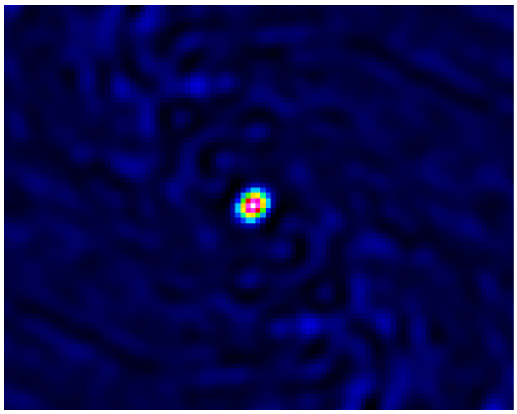

(a) Dirty Image

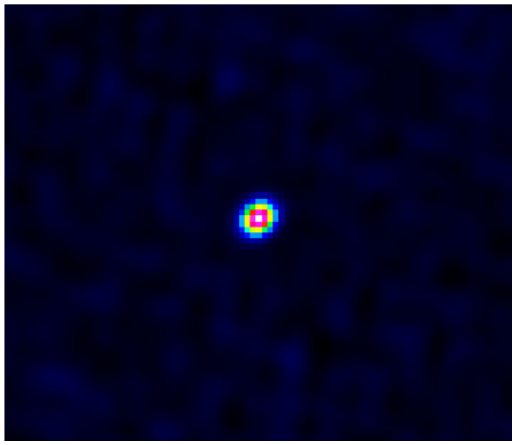

(b) Clean Image

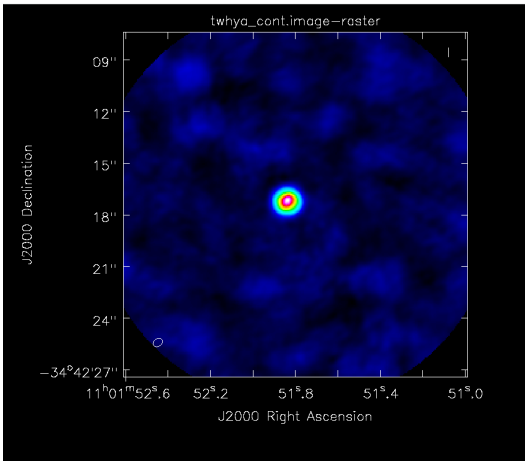

Figure 6.3: Continuum image

7. Markov Chain Monte Carlo

7.1 Motivation

Markov Chain Monte Carlo (MCMC) sampling is a powerful statistical method used in astronomy data analysis to explore complex and high-dimensional parameter spaces. It is particularly valuable when dealing with models that cannot be efficiently solved using traditional mathematical methods. MCMC sampling allows astronomers to infer the most likely set of parameters that best explain the observed data and obtain uncertainty estimates for those parameters.

7.2 Introduction

In statistics, Markov chain Monte Carlo (MCMC) is a class of algorithms used to draw samples from a probability distribution. Given a probability distribution, one can construct a Markov chain whose elements' distribution approximates it – that is, the Markov chain's equilibrium distribution matches the target distribution. The more steps that are included, the more closely the distribution of the sample matches the actual desired distribution.

Markov chain Monte Carlo methods create samples from a continuous random variable, with probability density proportional to a known function. These samples can be used to evaluate an integral over that variable, as its expected value or variance.

Practically, an ensemble of chains is generally developed, starting from a set of points arbitrarily chosen and sufficiently distant from each other. These chains are stochastic processes of "walkers" which move around randomly according to an algorithm that looks for places with a reasonably high contribution to the integral to move into next, assigning them higher probabilities.

Random walk Monte Carlo methods are a kind of random simulation or Monte Carlo method. However, whereas the random samples of the integrand used in a conventional Monte Carlo integration are statistically independent, those used in

MCMC are autocorrelated. Correlations of samples introduces the need to use the Markov chain central limit theorem when estimating the error of mean values. These algorithms create Markov chains such that they have an equilibrium distribution which is proportional to the function given.

7.3 Implementation

Our goal now is to fit the afterglow data of GW170817 with a smooth broken power law function as as shown

$$F(t,\nu) = 2^{1/s}\left(\frac{\nu}{3GHz}\right)^{\beta} F_p \left[\left(\frac{t}{t_p}\right)^{-s\alpha_1} + \left(\frac{t}{t_p}\right)^{-s\alpha_2}\right]^{-1/s} \tag{7.1}$$

where, F(t,ν) is the flux or intensity of the light curve at time t
F_p is the peak flux
t_p is the time at which the light curve reaches its peak
t is the time post merger
ν is the observing frequency, and β, α_1, α_2, s are model parameters.
Now the key steps for implementing MCMC sampling of data are:

- **Defining the model**: For example, here the model is a smooth broken power law for a light curve.
- **Define Priors**: Specify prior probability distributions for the model parameters that represent our knowledge or beliefs about the parameter values before seeing the data. In this case , I have used uniform or non informative priors for all the parameters.
- **Compute the likelihood**: Calculate the likelihood of the observed data given the model and its parameters. The likelihood represents how well the model explains the data. For example, in this case of a light curve, you would compute the likelihood by comparing the model light curve with the observed data points, considering the uncertainties in the data.
- **Define the Posterior Distribution**: Now Use Bayes' theorem to combine the prior probability distributions and the likelihood to obtain the posterior probability distribution of the model parameters given the observed data.
- **Running MCMC**: After initialising the parameter values and the no of walkers, run the MCMc algorithm for any number of steps (in this case 10000)
- **Visualisation**: Extract the optimal parameter values and plot the fitted graph.

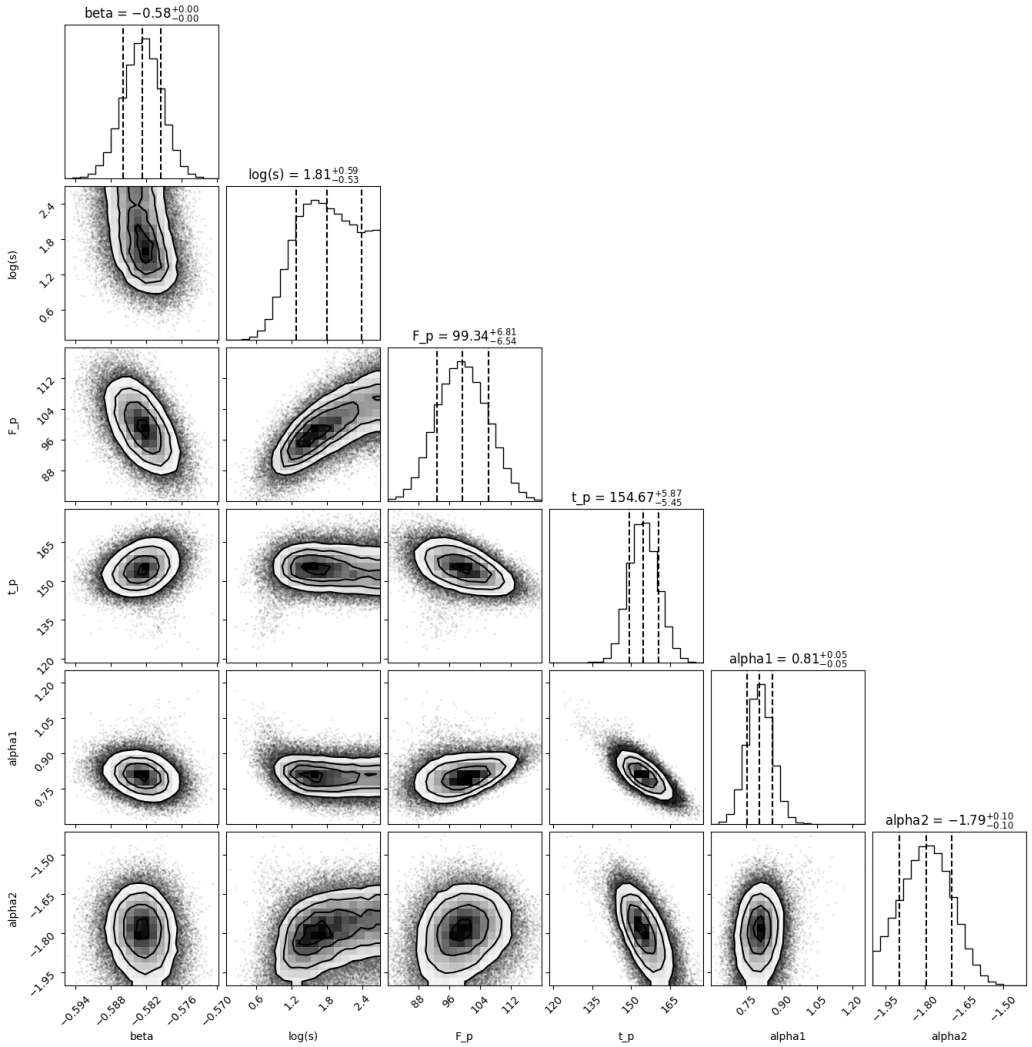

Figure 7.1: Corner plot showcasing the correlation between parameters which is similar to that shown in (5)

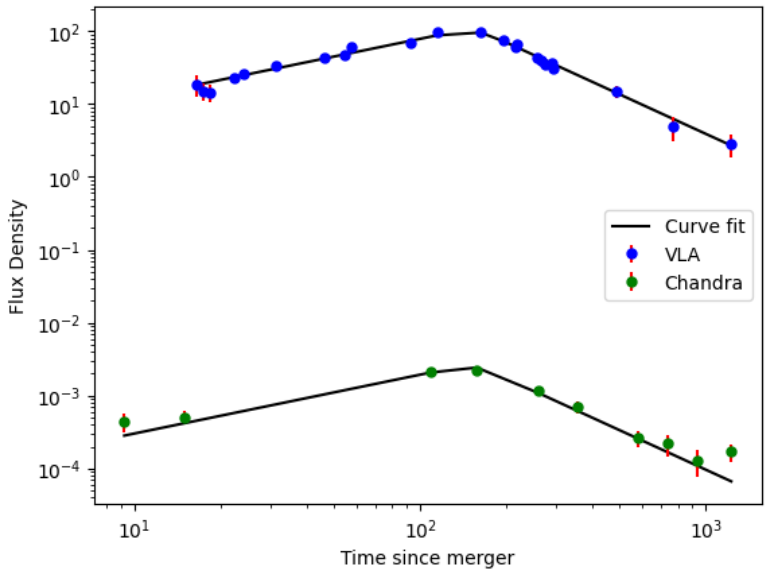

Figure 7.2: Obtained fit for VLA and Chandra data

Bibliography

(1) 1. *CIRADA Cutouts*. URL: http://cutouts.cirada.ca/help/ (cited on page 11).

(2) 2. *LIGO Caltech, GW170817 Press Release*. URL: https://www.ligo.caltech.edu/page/press-release-gw170817/ (cited on page 13).

(McM+07) J. P. McMullin et al. *CASA Architecture and Applications*. Edited by R. A. Shaw, F. Hill, and D. J. Bell. Oct. 2007 (cited on page 29).

(MSK15) J.M. Marr, R.L. Snell, and S.E. Kurtz. *Fundamentals of Radio Astronomy: Observational Methods*. ISSN. CRC Press, 2015. ISBN: 9781498770194. URL: https://books.google.co.in/books?id=T54oCwAAQBAJ (cited on page 7).

(Mak+21) S. Makhathini et al. "The Panchromatic Afterglow of GW170817: The Full Uniform Data Set, Modeling, Comparison with Previous Results, and Implications". In: *The Astrophysical Journal* 922.2 (Nov. 2021), page 154. ISSN: 1538-4357. DOI: 10.3847/1538-4357/ac1ffc. URL: http://dx.doi.org/10.3847/1538-4357/ac1ffc (cited on page 35).

Index

T